Downloaded from SAE International by Universita degli Studi di Modena, Wednesday, October 08, 2025

2025-24-0065 Published 07 Sep 2025

Analysis of Momentum Flux Distribution in Jets Produced by a Hydrogen Direct Injection System

Lucio Postrioti Università degli Studi di Perugia

Stefano Fontanesi Università di Modena e Reggio Emilia

Manuel Martino and Cristian Maka Università degli Studi di Perugia

Sebastiano Breda and Francesco Falcinelli Università di Modena e Reggio Emilia

Andrea Ricci Marelli Europe SpA

Citation: Postrioti, L., Fontanesi, S., Martino, M., Maka, C. et al., "Analysis of Momentum Flux Distribution in Jets Produced by a Hydrogen Direct Injection System," SAE Technical Paper 2025-24-0065, 2025, doi:10.4271/2025-24-0065.

Received: 12 May 2025 Revised: 25 Jun 2025 Accepted: 27 Jun 2025

Abstract

The adoption of hydrogen as carbon-free fuel for internal combustion engines in both transport and off-road applications could offer a significant contribution towards carbon neutrality. In the technical pathway to the conversion of conventional engines operating with liquid fuels to hydrogen, a key role is played by the injection systems. In particular for direct-injected combustion systems, the achievement of an adequate capability to control the gas jets development and the following mixing with air in the combustion chamber is mandatory in order to govern the heat release rate, so to obtain high efficiency levels while limiting the knock tendency and NOx formation. In order to achieve this complex task, injector caps featuring multiple holes (often non uniform in size) can be installed on the injector nozzle so to properly distribute hydrogen obtaining a proper matching with the combustion chamber design and with the air charge flow structure. To this end, the development of both appropriate simulation capabilities as well as effective diagnostic methodologies for a detailed characterization of high-pressure gas jets are required.

In the present paper, a single-hole GDI-derived prototype injector equipped with a 2-hole cap and fed with hydrogen is analysed with a combined experimental and 3D-CFD numerical methodology. The injector was characterized in terms of mean mass flow rate and global development of the two jets emerging from the cap. Further, the measurement of the momentum flux of the jets, coupled with the results of the 3D-CFD analysis, enabled the evaluation of the mass flow distribution among the two jets. The same 3D-CFD numerical tool, adequately validated with the available experimental data, was used to deepen the development of the flow structures within the injector cap, evidencing how the complex flow pattern inside the cap influences the evolution of the emerging jets. Globally, the combined experimental-numerical approach used was proved to be an effective methodology to support the development of hydrogen injection systems.

Introduction

In last years, the transportation sector – including on-and off-road, maritime and aviation applications - is experiencing a significant technical pressure as it is one of the largest sources of net CO_2 emissions, affecting the thermal balance of the planet. In this frame, a very challenging target of 2 °C as admittable increment for the global temperature has been set in the COP21 Conference [1], which was in particular implemented in the EU as a ban for fossil-fuelled new cars and light duty vehicles starting from 2035 [2]. In this not completely clear and still evolving legislation frame, internal combustion engines operated on non-fossil fuels such as hydrogen and synthetic hydrocarbons mixtures could play a significant role in achieving the targets of net CO_2 emissions, competing with the progressive electrification of the automotive sector. Following this path, an adequate "technological neutrality" among the different available options for vehicles powertrains (electrochemical batteries-based, hybrid thermal-electric and fuel-cell based) could be implemented, enabling a sort of natural selection in the search for the most efficient solution, including in the

Downloaded from SAE International by Universita degli Studi di Modena, Wednesday, October 08, 2025

analysis environmental, technical, economic and social benefits and costs.

In this complex and challenging scenario, green hydrogen-fuelled thermal powertrain is considered a promising solution [3], considering the virtually null CO_2 emission (if the effect of lubricant oil combustion is assumed as insignificant [4]) and the moderately challenging technological developments required for the use of hydrogen as fuel for a mature technology as ICEs. In detail, on-board hydrogen storage and management tasks (shared with fuel cell-based systems) are no longer significant issues, since adequate technologies have been developed and are available on the market [5, 6, 7]. In terms of thermodynamic behaviour, hydrogen fuelled engines have proved to offer satisfactory tank-to-wheel efficiency (around 40%), while the relatively low emission of thermal NOx produced by combustion can be abated with SCR aftertreatment or *ab origine* reduced to negligible levels adopting ultra-lean combustion strategies [8, 9]. In detail the required ultra-lean hydrogen combustion is enabled by both its very high laminar flame speed and wide flammability range, that allow the achievement of a stable combustion even with locally very high λ values. Despite the globally attractive potential related to the direct use of hydrogen as fuel in internal combustion engines, some development work needs to be fulfilled.

Reasonably, the development of appropriate hydrogen dosing and injection systems is one of the most significant technological barriers to be overcome. Hydrogen can be injected at low pressure in the intake system (PFI) or, at higher pressure, directly in the combustion chamber (HDI) after the intake valves closure. In both cases, the injection system must feature very high flow rate with respect to systems designed for liquid fuels, so to account for the reduced energy content per unit volume of hydrogen. Low pressure port injection favours the air/fuel charge homogenization, easing the combustion process control and reducing the risk of locally fuel rich parcels which can drastically increase NOx production. At the same time, PFI offer only a limited potential in terms of engine power density and efficiency, since the high volumetric fuel flow rate inhibits the achievement of high volumetric efficiency levels; finally, fuel port injection is exposed to the risk of backfire from the combustion chamber [10, 11]. In order to obtain high power density, the used of HDI is mandatory, significantly increasing the injection system complexity but also enhancing the possibility of controlling the air/fuel mixture formation and hence of managing the combustion process [12, 13, 14]. The high-pressure injection of hydrogen directly in the combustion chamber after the end of the intake process eliminates the risk of backfire without affecting the trapped air mass, thus enabling high BMEP and efficiency levels up to 45% at medium load. Further, the reduced fuel-air contact time tends to reduce pre-ignition and knock phenomena.

HDI systems operate at injection pressure levels in the range 20 to 60 bar as a compromise between opposite trends: higher pressure levels would shorten the injection process and simplify the injector design (higher mass flow rate per unit area of the flow section), enhancing the gas jet penetration and mixing capability in the combustion chamber; at the same time, very high injection pressure (up to 250-300 bar) would reduce the effective exploitation of the tank content, further stressing the onboard fuel storage issues. Consequently, the feasible injection pressure is moderate, and the crucial role of the gas jets in ensuring an adequate mixture formation process is evident: the fuel jet must quickly develop and propagate in the combustion chamber, with the jet's momentum flux the driving force available to promote the mixture formation in the compressed air. With the commonly used injection pressure levels in HDI systems, a pintle-hole nozzle configuration is used to ensure an adequate hydrogen flow section. As an alternative a large, multi-hole injector can be adopted. In both cases, a large gas column tends to develop downstream of the nozzle, hardly supporting an efficient mixing of the gas with the surrounding air. To promote the mixture formation, specific devices called “caps” are installed downstream of the nozzle; caps feature different large-bore holes designed to distribute the injected gas to different portions of the combustion chamber. Hence the operation of the cap becomes a crucial factor in determining the combustion quality, and its fluid-dynamic behaviour must be perfectly tuned with the combustion chamber needs. The critical role of hydrogen–air mixing within the combustion chamber in enhancing engine performance and reducing emissions is well established in recent literature. In particular, studies have shown that directing hydrogen jets toward preferential directions, leveraging the organized vortices within the cylinder, can significantly improve engine efficiency and output [15,16].

In this paper, a joint experimental and numerical 3D-CFD analysis of a HDI system equipped with a 2-hole cap and operated with hydrogen was carried out. The 2 holes feature significantly different flow sections in order to produce highly asymmetric gas streams in different portions of the downstream flow field. The cap is installed on a prototype, single hole injector provided by Marelli Europe and derived by a GDI unit. The flow rate capability of the tested unit was verified, assessing the intrusiveness of the cap with respect to the bare HDI injector. Further, the development of the two gas jets emerging from the cap holes was characterized by high-speed imaging using a Schlieren optical setup and the momentum flux pertaining to each single jet was measured. The obtained data were used for the tuning of the 3D-CFD numerical tool, by which both the complex flow inside cap and the flow rate pertaining to each of the jets in steady flow conditions was quantified, assessing the potential use of momentum flux as a measuring method to evaluate the mass distribution among the jets. The same integrated experimental-CFD approach evidenced a significant potential to investigate the root causes of the gas jets evolution and interaction with air charge flow structures, representing a robust tool to support the combustion system design.

Downloaded from SAE International by Universita degli Studi di Modena, Wednesday, October 08, 2025

Experimental Setup

In this study, a prototype hydrogen direct injector (HDI) developed by Marelli Europe was investigated. The injector is a solenoid type and features a spherical head needle with a single 0.65 mm diameter axial hole. As above described, single-hole or pintle-type hydrogen injectors are commonly coupled with nozzle caps designed with multiple holes to control the gas jets targeting within the combustion chamber. In this work, the injector was tested both as a standalone component and in combination with a custom-designed nozzle cap featuring two discharge holes (1 mm and 2 mm diameter), both inclined at 45° with respect to the injector axis and positioned along a cap diameter. The cap includes a tapping point to measure the internal pressure time-history during the injection events. The cap pressure signal was acquired using a piezoresistive pressure sensor (Keller PAA-M5-HB, 10 barA f. s.). Further geometrical details of the cap are provided in Figure 1.

Experimental tests were conducted using hydrogen supplied from a high-pressure cylinder (200 bar). A Coriolis-type mass flow meter (Siemens Mass2100) was installed downstream of the pressure regulator used to control the injection pressure level and upstream of a 100-cc volume rail feeding the injector. The large volume of the rail was designed in order to maintain approximately constant injection pressure during each event. A piezoresistive pressure sensor (Kistler 4005B, 100 barA full scale) was placed immediately upstream of the injector inlet to acquire the injection pressure time-history. The injector was actuated via a programmable driver (AEA A006) using a peak-and-hold current profile recorded during the campaign with a current clamp. The injector was installed on a closed test vessel featuring two 100 mm diameter opposed optical accesses, with the vessel kept at ambient pressure during the tests and rendered inert by injection into nitrogen gas.

FIGURE 1 Mounting configuration and cap section with two outlet holes of 1 mm and 2 mm diameter and the tapping point.

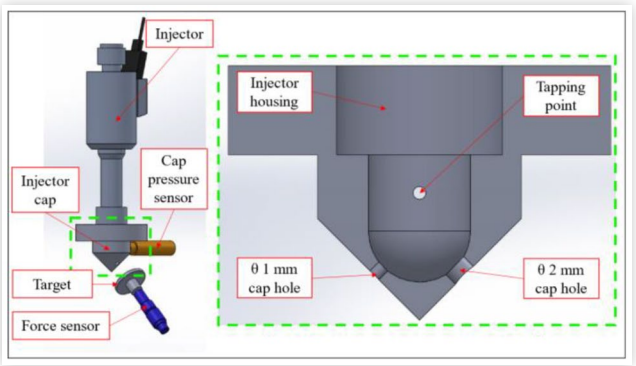

The experimental campaign (see Table 1) included the following tests:

TABLE 1 Test plan.

General conditions				
Case	P_{inj} [barA]	T_{inj} [K]	P_{vessel} [barA]	P_{inj}/P_{vessel}
A	20	293	1	20
B	40	293	1	40
Mean Mass Flow Rate				
ET [ms]				
0.45; 0.5; 0.7; 1.0; 2.0; 4.0; 6.0				
Schlieren Imaging				
ET [ms]	Resolution [px x px]	Resolution [px/mm]	Exposure time [µs]	Frame rate [fps]
6	705 x 656	6.6875	1	10000
Momentum flux				
ET [ms]	Target diameter [mm]		Target-hole distance [mm]	
6	14		10	

- Measurement of mean mass flow rate by varying the injector energizing time, and derivation of EMI curves (energizing time *vs.* mean injected mass).
- Schlieren imaging of hydrogen jets.
- Measurement of single jet's momentum flux.

All the tests were conducted at two injection pressure levels: 20 barA and 40 barA. The injection pressure level range was chosen in order to be representative of medium pressure, direct injection system currently under development for automotive applications. The tested injector logic command durations ranged from ballistic to fully-linear injector operation. Measurements were carried out using the injector both with and without the nozzle cap.

The EMI curves were acquired actuating the injector at frequencies ranging from 10 to 50 Hz (higher for smaller injected quantities), with a minimum of 500 shots per ET value. This EMI curves, as typical for GDI injection systems, exhibit an initial nonlinear (ballistic) region, where the ET is shorter than the time required for the needle to reach its maximum lift. In this condition, the needle remains floating for the entire duration of the event, leading to greater shot-to-shot dispersion of the injected volume [17]. For longer ET values, the needle achieves a steady-state lift and the injector operates in the so-called linear regime.

To analyse the evolution of the hydrogen jets emerging from the nozzle or from the cap holes under varying conditions, Schlieren high-speed imaging was applied. This technique visualizes gas jets by exploiting refractive index gradients between the jet and the surrounding medium. A Schlieren optical bench in a Z-configuration was used (Figure 2), with high-speed videos captured by a Phantom Vision Research 7.10 camera, operated acquiring 704 x 656 pixels images at a frame rate of 10000 fps. The exposure time was set to 1 µs. The camera was equipped with a 200 mm Nikkor

Downloaded from SAE International by Universita degli Studi di Modena, Wednesday, October 08, 2025

FIGURE 2 schematic of the Schlieren imaging setup.

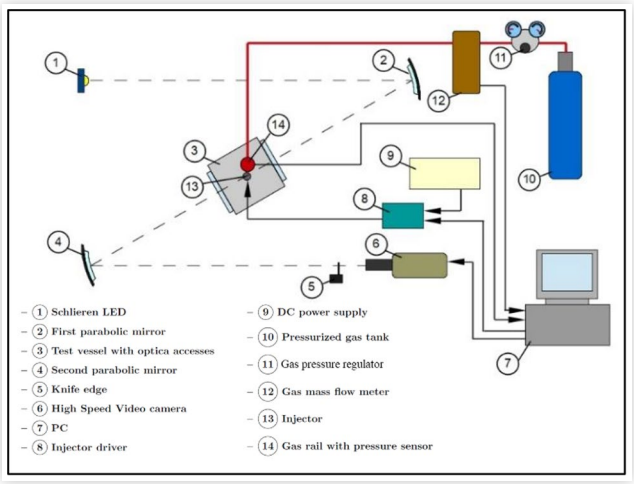

lens. The spatial resolution achieved was 6.6875 pixels/mm; in each operating condition, 20 acquisitions of the evolving jets were acquired. The recorded videos were post-processed to extract the overall geometric parameters of the jets (penetration length, cone angle and bend angle relative to the injector axis). Jet contours were obtained by applying a threshold to the standard deviation of pixel intensity values. More details about the image acquisition and post-processing procedures are reported in [18].

The global momentum flux of the jets was determined by measuring the impact force exerted by the jet when impacting on a circular target (diameter: 14 mm) mounted on a piezoelectric force sensor (Kistler 9215A). Depending on the configuration, the force was measured for the single jet exiting the nozzle or separately for the two jets exiting the cap holes. In all cases, the target was positioned orthogonally to the jet nominal axis at a fixed distance of 10 mm from the cap outlet section (see Figure 1). Both the target diameter and its distance from the nozzle hole were selected based on a previous sensitivity analysis [19] and were kept constant across all experimental conditions to ensure consistency. In particular, the target diameter was chosen to ensure both a complete interaction with the jets under all operating conditions while minimizing the onset of secondary flow vortexes affecting the measurement during the jet-target impact transient.

Numerical Setup

The same experimental configuration, comprising a single-hole injector coupled with a two-hole cap, is replicated with CFD simulations to further investigate the outcomes of the experimental campaign. The numerical setup employed follows a methodology previously validated by the authors in earlier studies on the same injector [18, 19, 20], and more recently applied to a pintle injector equipped with a single-hole cap [21]. For the sake of completeness, the methodology is briefly summarized here, while full details are available in the referenced publications.

In the preliminary numerical analysis, steady-state simulations are conducted within a RANS framework, thereby neglecting transient effects related to injector opening and closing. The regime condition is modelled using the CFD software STAR-CCM+ (v2310), licensed by SIEMENS DISW. Due to the axisymmetric geometry of the injector/cap assembly, only half of the physical domain is simulated, employing a symmetry plane that passes through the injector axis and bisects the cap holes. The computational domain also includes the cylindrical test vessel.

A fixed, trimmed mesh is generated, with additional refinement applied in regions of particular interest for flow characterization—namely, the nozzle tip, injector hole, cap holes, and the zone where the gas jets evolve. Volumetric cylindrical and conical refinement zones are introduced to enhance mesh resolution in these critical areas. Furthermore, 15 to 25 near-wall layers are implemented to maintain a Y^+ value below 1, in accordance with the selected wall treatment approach. A schematic of the mesh, which consists of approximately 5 million cells for the half-domain configuration, is shown in Figure 3 for illustrative purposes.

Special consideration is given to defining both background and injected gas properties as functions of pressure and temperature, using the Soave–Redlich–Kwong real gas equation of state [22] instead of the commonly used ideal gas law. This choice accounts for the high pressures and temperatures characteristic of under-expanded gas jets. A coupled flow solver employing a second-order discretization scheme is used to resolve the flow, energy, species transport, and turbulence. The Realizable k–ε turbulence model is adopted. At the inlet boundary, the experimentally measured static mass flow rate is imposed, ensuring consistency and accuracy by confirming that the inlet pressure aligns with the measured rail pressure.

Experimental Results

The present section reports the main outcomes of the experimental investigation. During the experimental campaign, the pressure history within the rail was recorded for all operating conditions. When applicable, the static pressure profile inside the jet cap was also acquired. Figure 4 presents the injector current signal, the upstream pressure in the 100-cc rail and the internal cap pressure during an injection event characterized by a command duration of 6.0 ms.

The storage volume was sufficiently large to limit pressure drop, resulting in a pressure reduction of approximately 0.13 bar at 20 barA injection pressure and 0.22 bar at 40 barA. As a consequence of hydrogen injection, the internal cap pressure exhibited a transient increase, reaching steady-state values of 2.74 barA and 1.53 barA for injection pressures of 40 barA and 20 barA,

Downloaded from SAE International by Universita degli Studi di Modena, Wednesday, October 08, 2025

FIGURE 3 Schematic and details of the employed numerical grid. In the red boxes absolute mesh size in the refinement regions is reported.

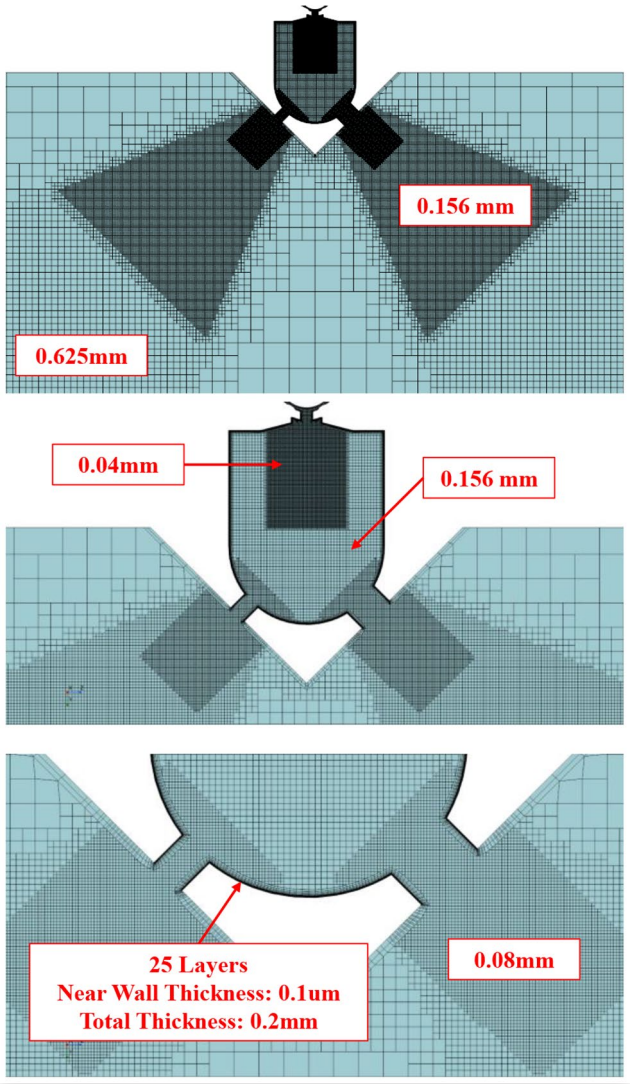

respectively. In the first case, the cap operates under choked flow conditions, as the ratio between the internal pressure and the ambient pressure exceeds the critical pressure ratio. In the second case, the pressure ratio across the cap holes does not fully attain the critical ratio, and therefore the resulting outflow will be presumably in a transition across critical conditions. As can be observed in Figure 4, the cap pressure initial rise occurs with 0.5 ms delay with respect to the time reference (coincident with the electric command start), sensing the start of the injection process. The same event is almost simultaneously detected by the rail pressure sensor in terms of pressure decay, with an additional small propagation delay related to higher distance of the rail sensor from the needle seal. The cap pressure attains a steady level within 1.5 ms from the command start, which is maintained up to 6.75ms suggesting the needle closure start. Later, some pressure peaks in the cap seem to indicate the occurrence of needle bounces, as also suggest by

FIGURE 4 Current profile, rail pressure and cap internal pressure for both injection pressure level (20 barA and 40 barA).

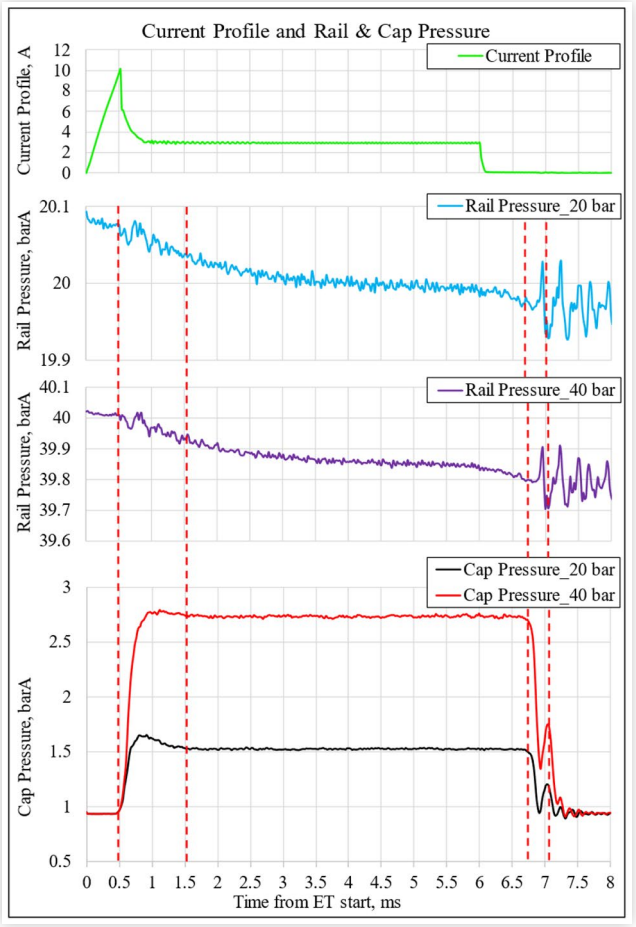

corresponding pressure pulsations in the rail and by the acquired images.

The results of the flow rate analysis under the tested conditions are presented in Figure 5, expressed as milligrams of hydrogen injected per shot as a function of the energizing time (ET). For ET values below 1 ms, the injector operates in its so-called ballistic regime, while for longer energizing times, the injector exhibits a linear response. In the linear region, the steady-state mass flow rate can be calculated from the slope of the curves, obtaining values of 0.33 g/s and 0.66 g/s for injection pressures of 20 barA and 40 barA, respectively. Flow characterization tests indicate that the injector's mass flow rate shows only minor differences between configurations with and without the jet cap. This behavior is attributed to the establishment of choked flow conditions within the injector, under which the flow rate is determined only by upstream conditions and becomes independent of downstream pressure. With the used cap, the flow is hence controlled by the injector itself. Furthermore, the measured flow rates are consistent with the expected values reported in a previous study [18], where hydrogen flow rate estimations for the same injector were based on flow tests obtained using surrogate gases (helium, nitrogen, argon).

Downloaded from SAE International by Universita degli Studi di Modena, Wednesday, October 08, 2025

FIGURE 5 EMI curves for both configurations, with and without jet cap and for each pressure level.

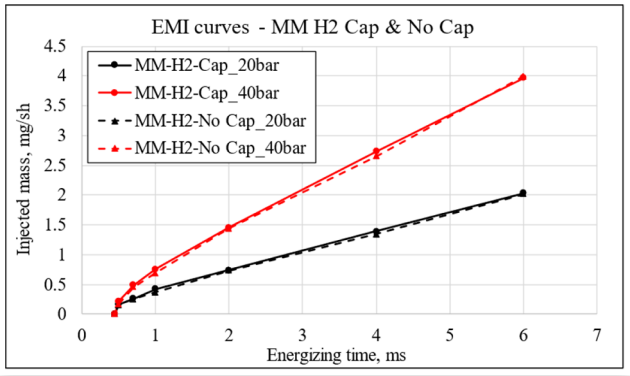

A geometrical characterization of the hydrogen jets was conducted based on Schlieren imaging. Figure 7 illustrates a sequence of jet images for configurations with and without the jet cap. For the sake of brevity, only the case corresponding to the 40 barA injection pressure is presented. From the Schlieren contours, jet penetration, cone angle, and bend angle were quantified for both configurations. Jet penetration was defined (Figure 6) as the axial distance of the jet contour tip from the nozzle exit along a line perpendicular to the orifice outlet section. The cone angle was determined as the angle between the fitting lines to the left and right jet boundaries, while the bend angle was defined as the inclination between the cone angle bisector and the injector axis.

The outcomes of this analysis for injection pressures of 20 barA and 40 barA are reported in Figure 8 and Figure 9, respectively. The results indicate that the presence of the cap drastically reduces the jet penetration

FIGURE 6 Jet structure: definition of tip penetration, cone angle and bend angle.

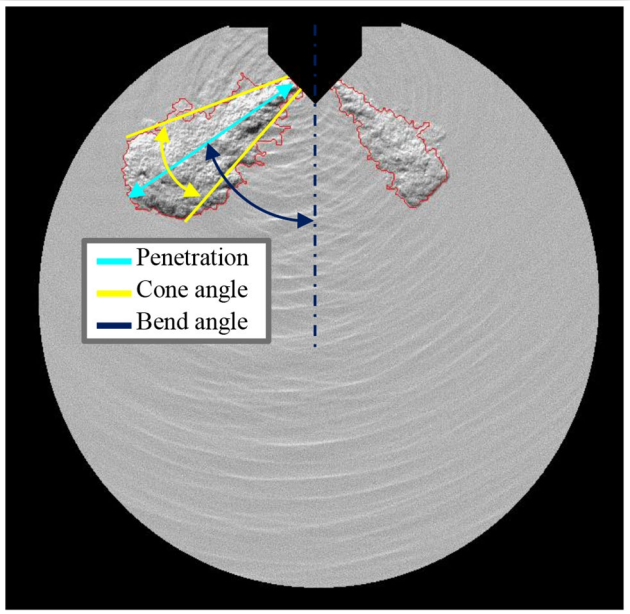

FIGURE 7 Schlieren images of jets evolution. Comparison between jets behaviour in presence of cap and jet without cap in 40 barA case.

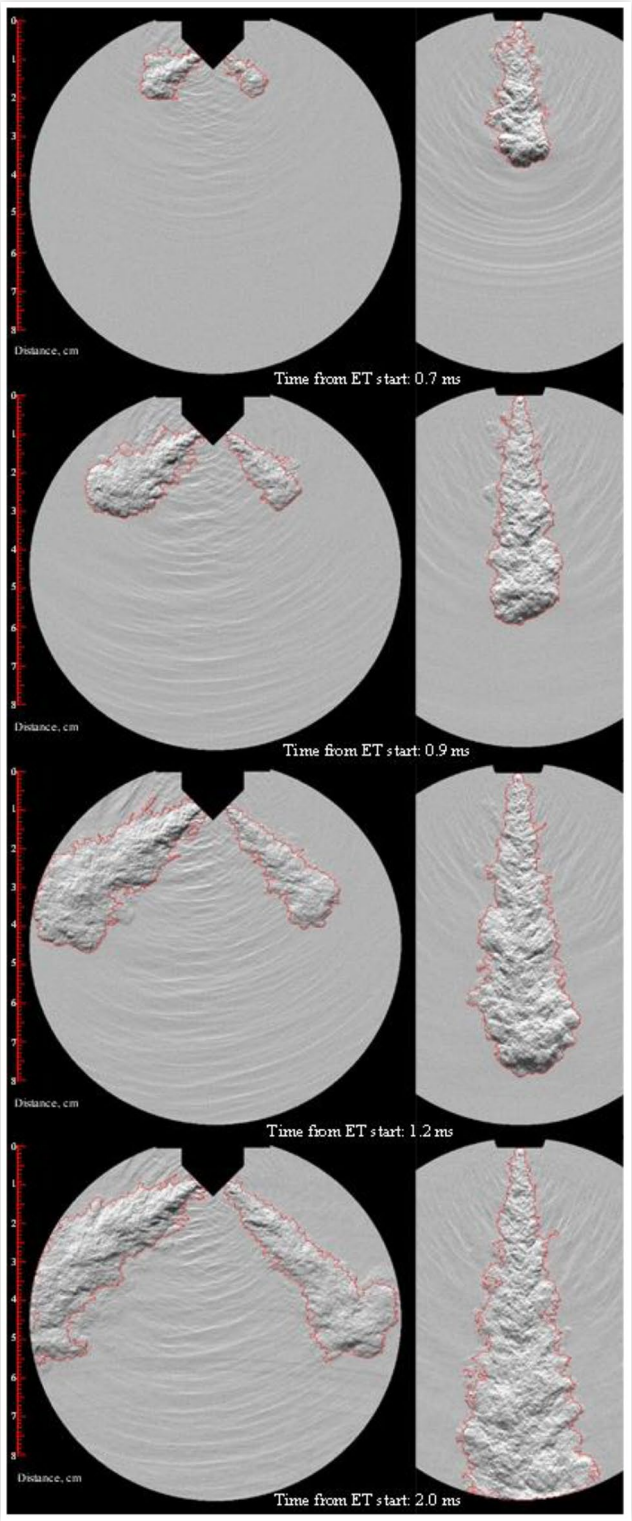

into the test vessel compared to the bare injector configuration. Additionally, the jet produced from the 2 mm orifice exhibits initially a significantly greater penetration than that from the 1 mm orifice, both at 40 barA where sonic conditions are fully reached within the cap, and at 20 barA, where the flow through the cap remains in transition

Downloaded from SAE International by Universita degli Studi di Modena, Wednesday, October 08, 2025

FIGURE 8 Penetration, cone angle and bend angle in 20 barA case for both configuration with and without jet cap.

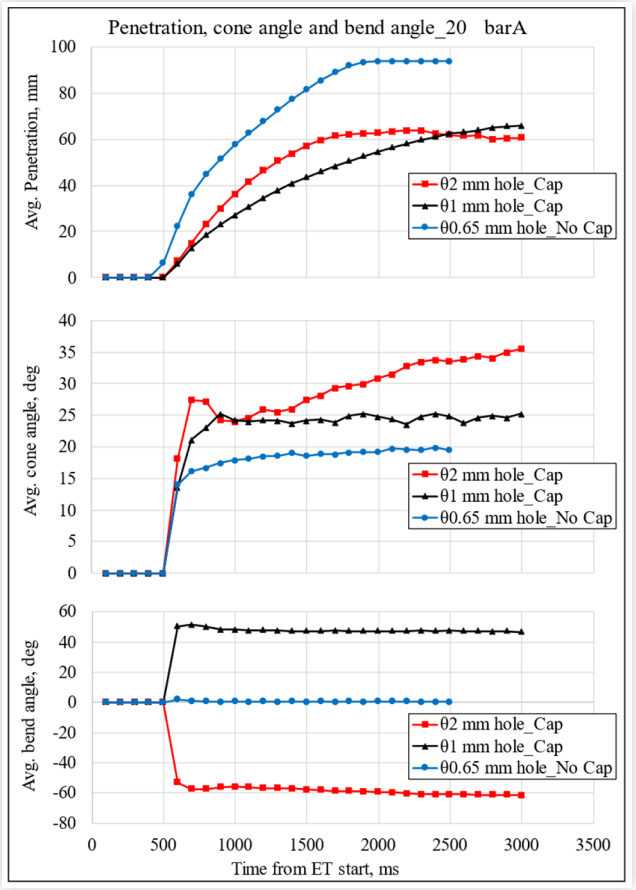

FIGURE 9 Penetration, cone angle and bend angle in 40 barA case for both configuration with and without jet cap.

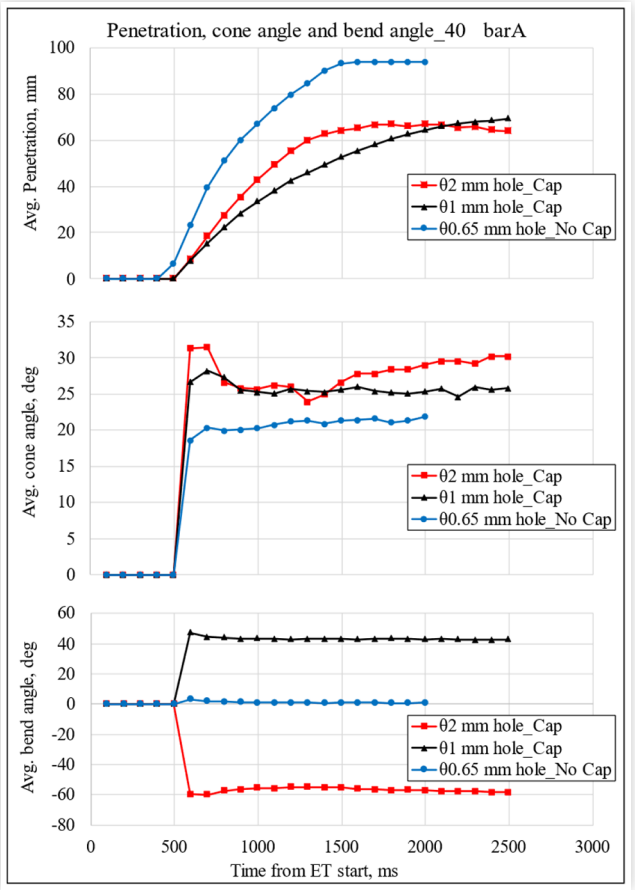

between subsonic and fully sonic. The images analysis evidences how the drag effect exerted by quiescent nitrogen on the hydrogen jet emerging from the 1-mm hole is higher than for the other jet. This can be considered an effect of its larger surface area to jet volume (and hence to momentum flux) ratio with respect to the jet produced by the 2-mm hole, resulting in a slower jet tip penetration in the test vessel. The cone angle measured from images is larger for jets exiting the cap compared to the bare injector jet, with the widest angle observed for the jet from the larger (2 mm) cap orifice. The acquired videos for the 2-mm-hole jet suggest a slight oscillation of the flow direction close to the hole exit section, resulting in a progressively growing cone angle. Conversely this parameter remains stable during the injection process for the jet fed by the 1 mm-hole. As suggested by the following 3D-CFD analysis, these different jet behaviours could be due to the complex flow structure in the nozzle cap, with the 2-mm hole being fed by to distinct and conflicting gas streams (Figure 14). For the no-cap configuration, the jet exhibited negligible bend angles (0.55 deg and 1.12 deg) while the jets emerging from the cap showed final bend angles around - 60 and - 58 deg for the 2 mm orifice, compared to a nominal angle of - 45 deg, and about 44 and 42 deg for the 1 mm orifice, compared to a nominal angle of 45°, at 20 barA and 40 barA, respectively. The obtained deviations from the nominal values suggest a complex flow pattern in the spray cap, affecting the final jets targeting.

Figure 10 and Figure 11 present the momentum flux trends, measured as the impact force of the jets from the cap orifices on the target surface; in the same figures, the cap pressure signal is reported as refence. For confidentiality reasons, momentum values have been reported in relative terms. The plots show that, under steady-state

FIGURE 10 Cap pressure and hole momentum contribution curve for 20 barA injection pressure case.

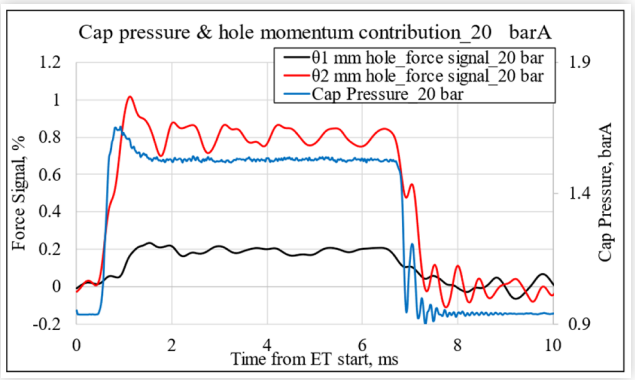

Downloaded from SAE International by Universita degli Studi di Modena, Wednesday, October 08, 2025

FIGURE 11 Cap pressure and hole momentum contribution curve for 40 barA injection pressure case.

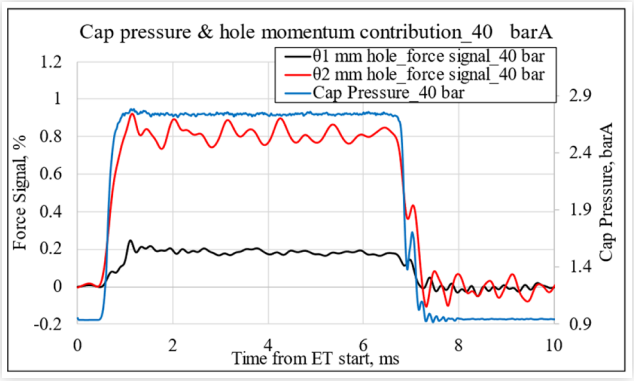

FIGURE 12 Comparison between Experimental Momentum ratio (1mm hole/2 mm hole) and CFD derived mass flow rate ratio (1mm hole/2 mm hole). If ideal, a 25% split, equal to area ratio is expected.

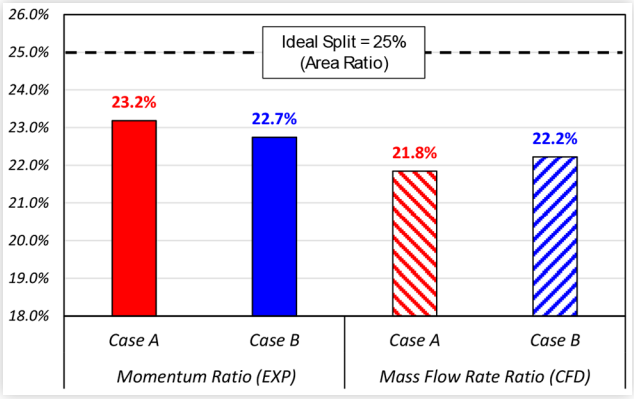

conditions, the jet from the larger orifice contributes 81.2% and 81.5% of the total measured momentum at 20 barA and 40 barA, respectively, compared to a nominal contribution of 75% expected considering the ratio of the respective geometrical flow sections. The ratio of the momentum flux contribution from the smaller orifice to that of the larger orifice is 23.2% and 22.7% at 20 barA and 40 barA, respectively (see Figure 12). Assuming equal exit velocities for both jets, these ratios correspond to the mass flow rate ratio between the two orifices. Therefore, important information about the distribution of fuel within the combustion chamber can be obtained from the momentum flux measurement. Further, it is interesting to observe how the post injection events, detected in terms of cap pressure final oscillations, are also sensed in terms of momentum flux at the end of the injection process.

Preliminary CFD Analyses

The first insight provided by the CFD simulation is the mass flow distribution between the two injector cap holes, which cannot be directly measured experimentally. However, an indirect estimation is possible through the measurement of momentum flux. Based on the geometric area ratio of 25% between the two holes, an ideal mass flow split of 80%-20% in favour of the larger hole is expected. In practice, however, this ideal distribution may not be achieved due to the complexities of the internal cap flow.

Experimental measurements of the momentum flux through the holes reveal a slightly higher-than-expected force from the larger (2 mm-diameter) hole, suggesting more effective utilization of the larger passage. This is supported by the observed force ratio between the smaller (1 mm-diameter) and larger hole (2 mm diameter), which is approximately 23%, lower than the expected 25%, at both tested injection pressures.

CFD results further validate this observation, predicting a mass flow split of 82%-18% (≈22%) in favour of the larger hole, indicating a 3% deviation from the ideal case. This comparison, illustrated in Figure 12, confirms the effectiveness of momentum flux measurements in assessing the mass flow distribution between the cap holes and validate the CFD simulation results.

Further analysis of the CFD results, particularly the internal cap flow field, provides insight into the causes of the non-ideal mass flow split between the two injector holes. As shown in Figure 13, a clear asymmetry is observed in the flow structure, with the hydrogen jet from the injector exhibiting a deviation toward the larger (2 mm-diameter) hole. This preferential flow direction results in uneven utilization of the available cross-sectional areas, contributing to the observed mass flow imbalance. Additionally, this asymmetric behaviour influences the external jet characteristics, notably causing measurable differences in the jet bend angles between the two holes.

The impingement of the jet on the internal surfaces of the injector cap generates a counter-clockwise rotating vortex, which significantly influences the internal flow distribution and results in asymmetric feeding of the two holes. Specifically, the smaller hole is supplied primarily by a single stream originating from the bottom region of the cap. In contrast, the larger hole receives flow from two distinct directions: one from the bottom and another from the top of the cap. This dual feeding mechanism enables more effective utilization of the 2 mm-diameter hole's cross-sectional area and contributes to the

FIGURE 13 Velocity Magnitude field inside the cap. Orthogonal views.

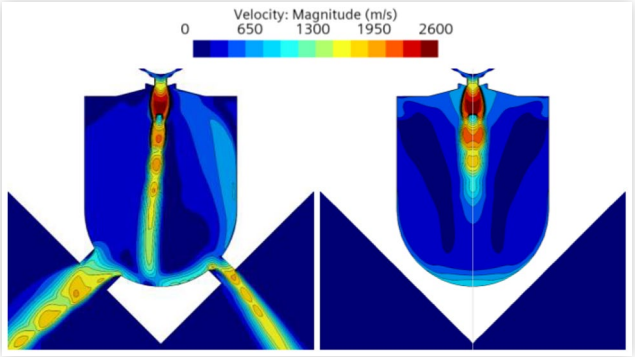

Downloaded from SAE International by Universita degli Studi di Modena, Wednesday, October 08, 2025

observed imbalance in the mass flow distribution. This difference in flow feeding is clearly illustrated by the internal streamlines shown in Figure 14.

As previously discussed, the internal flow field within the cap and the asymmetric feeding of the holes are key factors influencing the observed differences in jet bending angles. This effect is evident in the Schlieren images, where the jet issuing from the 1mm-diameter hole exhibits a smaller bend angle compared to that from the 2mm-diameter hole. The reduced deflection is attributed to the flow deviation within the smaller hole, which directs the jet closer to the injector axis. This interpretation is further supported by the post-processed results shown in Figure 15, where the reduced bend angle and inward flow deviation from the smaller hole are clearly visible. In the picture (Figure 15) a hydrogen mass fraction based iso-surfaces (set to 0.05) is adopted to distinguish the H_2 jets from the background. Differences in the absolute values of the bend angle between experimental (Figure 9) and numerical results (Figure 15) are mainly due to the changing direction of the jet development during the onset transient, which cannot be captured by the steady flow simulation while it is accounted for in the image analysis procedure. Further insight into this aspect could be achieved through the analysis of momentum flux distribution within each single jet. Nevertheless, the trend predicted by the numerical simulation is consistent with the experimental observations, supporting the validity of the analysis performed.

FIGURE 14 Streamlines inside the cap.

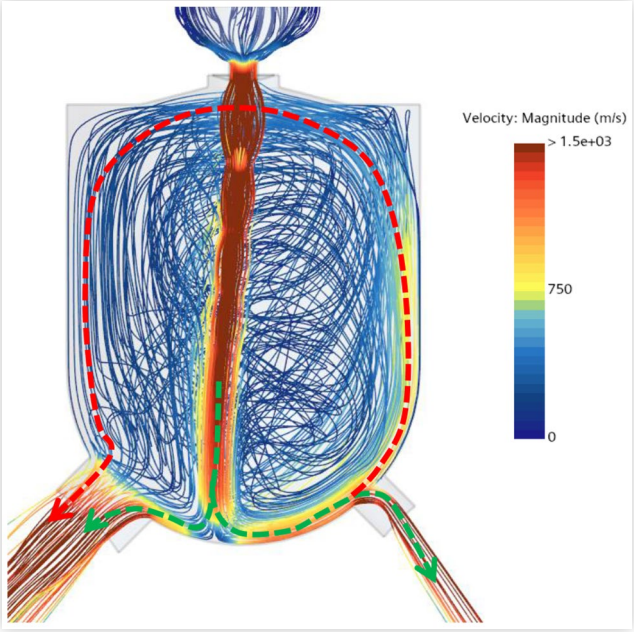

FIGURE 15 Evolution of the H_2 jets outside from the cap. The lower bending angle from the 1-mm hole jet is clearly visible as a consequence of the inner cap flow field.

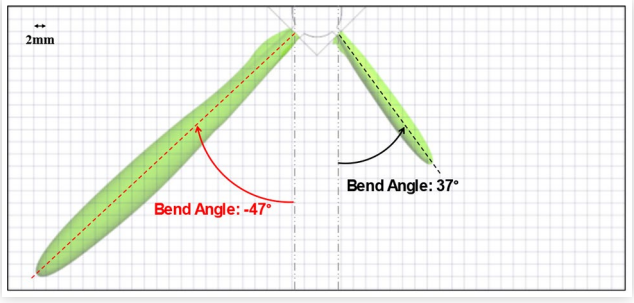

Conclusions

In the present work, the operation of a prototype, high-pressure injector for hydrogen applications was investigated using a combined experimental and 3D-CFD numerical approach. The analysed operating conditions included the use of hydrogen injected at 20 and 40 bar, with injector command durations covering both ballistic and linear operation. For hydrogen direct-injected engines, the use of caps installed on the nozzle is considered one of the most promising options to control the hydrogen-air charge interaction so to guide the combustion process evolution. The injector under test was hence equipped with a two-hole, different diameter cap in order to investigate the potential capability of this kind of design to effectively control the actual targeting of the hydrogen jets. The experimental analysis was carried out in terms of overall flow characteristics of the examined injector configurations. A Schlieren imaging methodology was used to investigate the global evolution of the two jets emerging from the cap compared with the single jet produced by the bare injector. Further, the momentum flux of the two jets was individually measured, in order to estimate the actual mass flow distribution among them. The numerical analysis was mainly used as a means to investigate non-measurable quantities, such as the flow structure inside the cap and the contributions of the jets emerging from the cap in terms of mass flow rate.

In the following, the main evidences obtained from the present research are summarised:

- The flow rate measurement confirmed that the tested configuration with cap does not affect the flow capability of the injector in all the tested operating conditions, being the mass flow rate controlled by the injector needle.
- The imaging analysis of the hydrogen jets confirmed the capability of the examined cap configuration to produce well-separated jets, that can be conveniently targeted to specific portions of the combustion chamber. The actual targeting was proved to be somewhat different from the expected one, suggesting the presence of complex flow structures in the cap.
- The momentum flux measurement of the two jets showed a ratio of the respective contributions to the total momentum flux produced by the injection system slightly different from the expectations, confirming the importance of a deep analysis of the in-cap flow.

Downloaded from SAE International by Universita degli Studi di Modena, Wednesday, October 08, 2025

- The 3D-CFD analysis revealed asymmetric flow in the cap, resulting here in the formation of a main reverted vortex feeding the two holes. As a result, the sections of discharge channels are differently exploited, with the emerging jets deviating from the nominal directions as also seen in the experimental analysis.

Overall, the joint use of numerical and experimental approaches allowed us to obtain a deep insight in the operation of the tested hydrogen injection system, validating this approach in supporting injection system design.

References

1. Paris Agreement, n.d., accessed April 20, 2025, https://climate.ec.europa.eu/eu-action/international-action-climate-change/global-climate-action_en.
2. "Regulation (EU) 2023/851 of the European Parliament and of the Council of 19 April 2023 Amending Regulation (EU) 2019/631 as Regards Strengthening the CO2 Emission Performance Standards for New Passenger Cars and New Light Commercial Vehicles in Line with the Union's Increased Climate Ambition (Text with EEA Relevance)," vol. 110. 2023.
3. Baade, W.F., Parekh, U.N., and Raman, V.S., *Hydrogen. Kirk-Othmer Encyclopedia of Chemical Technology* (John Wiley & Sons, Ltd, 2001), doi:https://doi.org/10.1002/0471238961.0825041803262116.a01.pub2
4. Boretti, A., "Hydrogen Internal Combustion Engines to 2030," *International Journal of Hydrogen Energy* 45, no. 43 (2020): 23692-23703, doi:https://doi.org/10.1016/j.ijhydene.2020.06.022.
5. Rivard, E., Trudeau, M., and Zaghib, K., "Hydrogen Storage for Mobility: A Review," *Materials* 12 (2019): 1973, doi:https://doi.org/10.3390/ma12121973.
6. Okonkwo, P.C., Barhoumi, E.M., Ben Belgacem, I., Mansir, I.B. et al., "A Focused Review of the Hydrogen Storage Tank Embrittlement Mechanism Process," *International Journal of Hydrogen Energy* (2023), doi:https://doi.org/10.1016/j.ijhydene.2022.12.252.
7. Li, H., Cao, X., Liu, Y., Shao, Y. et al., "Safety of Hydrogen Storage and Transportation: An Overview on Mechanisms, Techniques, and Challenges," *Energy Reports* 8 (2022): 6258-6269, doi:https://doi.org/10.1016/j.egyr.2022.04.067.
8. Dimitriou, P. and Tsujimura, T., "A Review of Hydrogen as a Compression Ignition Engine Fuel," *Int. J. Hydrog. Energy* 42, no. 38 (2017): 24470-24486, doi:10.1016/j.ijhydene.2017.07.232.
9. Takagi, Y., Oikawa, M., Sato, R., Kojiya, Y. et al., "Near-Zero Emissions with High Thermal Efficiency Realized by Optimizing Jet Plume Location Relative to Combustion Chamber Wall, Jet Geometry and Injection Timing in a Direct-Injection Hydrogen Engine," *Int. J. Hydrog. Energy* 44, no. 18 (2019): 9456-9465, doi:10.1016/j.ijhydene.2019.02.058.
10. Cheng, X., Baigang, S., and Zhen, H., "Investigation on Jet Characteristics of Hydrogen Injection and Injection Strategy for Backfire Control in a Port Fuel Injection Hydrogen Engine," *Energy Procedia* 105 (2017): 1588-1599, doi:https://doi.org/10.1016/j.egypro.2017.03.508.
11. Gao, J., Wang, X., Song, P., Tian, G. et al., "Review of the Backfire Occurrences and Control Strategies for Port Hydrogen Injection Internal Combustion Engines," *Fuel* 307 (2022): 121553, doi:https://doi.org/10.1016/j.fuel.2021.121553.
12. Yip, H.L., Srna, A., Yuen, A.C.Y., Kook, S. et al., "A Review of Hydrogen Direct Injection for Internal Combustion Engines: Towards Carbon-Free Combustion," *Applied Sciences* 9 (2019): 4842, doi:https://doi.org/10.3390/app9224842.
13. Li, Y., Gao, W., Zhang, P., Fu, Z. et al., "Influence of the Equivalence Ratio on the Knock and Performance of a Hydrogen Direct Injection Internal Combustion Engine under Different Compression Ratios," *International Journal of Hydrogen Energy* 46 (2021): 11982-11993, doi:https://doi.org/10.1016/j.ijhydene.2021.01.031.
14. Tanno, S., Ito, Y., Michikawauchi, R., Nakamura, M. et al., "High-Efficiency and Low-NOx Hydrogen Combustion by High Pressure Direct Injection," *SAE Int. J. Engines* 3, no. 2 (2010): 259-268, doi:https://doi.org/10.4271/2010-01-2173.
15. Goyal, H., Jones, P., Bajwa, A., Parsons, D. et al., "Design Trends and Challenges in Hydrogen Direct Injection (H2DI) Internal Combustion Engines – A Review," *International Journal of Hydrogen Energy* 86, no. 11 (2024): 1179-1194, doi:https://doi.org/10.1016/j.ijhydene.2024.08.284ù.
16. Breda, S., Patrizi, V., Berni, F., and Tonelli, R., "Computational Study of Injector Cap Design for Optimized Mixing and Combustion in a High-Performance DI Hydrogen Engine," *International Journal of Hydrogen Energy* 138 (2025): 129-15016, doi:https://doi.org/10.1016/j.ijhydene.2025.05.085.
17. Cavicchi, A. and Postrioti, L., "Simultaneous Needle Lift and Injection Rate Measurement for GDI Fuel Injectors by Laser Doppler Vibrometry and Zeuch Method," *Fuel* 285 (2021): 119021, doi:https://doi.org/10.1016/j.fuel.2020.119021.
18. Breda, S., Magnani, M., Martino, M., Fontanesi, S. et al., "Experimental and Numerical Characterization of a Single-Hole Lpdi Hydrogen Injector: Identification of a Suitable Inert Replacement for Hydrogen Jet Studies," *Fuel* 399 (2025): 135626, doi:https://doi.org/10.1016/j.fuel.2025.135626.
19. Postrioti, L., Martino, M., Fontanesi, S., Breda, S. et al., "Experimental and Numerical Momentum Flux Analysis of Jets from a Hydrogen Injector," SAE Technical Paper 2024-01-2616 (2024), doi:10.4271/2024-01-2616.
20. Fontanesi, S., Postrioti, L., Magnani, M., Martino, M. et al., "Preliminary Assessment of Hydrogen Direct Injection Potentials and Challenges through a Joint Experimental and Numerical Characterization of High-Pressure Gas Jets," SAE Technical Paper 2022-24-0014 (2022), doi:https://doi.org/10.4271/2022-24-0014.

Downloaded from SAE International by Universita degli Studi di Modena, Wednesday, October 08, 2025

21. Pavan, N., Cicalese, G., Gestri, L., Fontanesi, S. et al., "Effects of Jet Caps on Hydrogen Piezoelectric Injectors for DI Applications: Experiments and 3D-CFD Simulations," SAE Technical Paper 2025-01-8454 (2025), doi:10.4271/2025-01-8454.

22. Soave, G., "Equilibrium Constants from a Modified Redlich-Kwong Equation of State," *Chemical Engineering Science* 27 (1972): 1197-1203, doi:https://doi.org/10.1016/0009-2509(72)80096-4.

Acknowledgments

Marelli Europe is kindly acknowledged for supporting the research activity with the development of the prototype injector.

Sebastiano Breda and Stefano Fontanesi acknowledge the financial support provided by by "European Union- Next generation EU trough the "PIANO NAZIONALE DI RIPRESA E RESILIENZA (PNRR) – MISSION 4 COMPONENTE 2, "Dalla ricerca all'impresa" INVESTIMENTO 1.4, (CN00000023). In the context of the "Sustainable Mobility Center (Centro Nazionale per la Mobilità Sostenibile – CNMS)" - Spoke 12 - Avviso MUR 3138/2021 modificato con DD 3175/2021"

Definitions/Abbreviations

CFD - Computational Fluid Dynamics

EMI - Einspritz Mengen Indikator (Injection Quantity Indicator)

ET - Energizing Time, ms

HDI - Hydrogen Direct Injection

ICE - Internal Combustion Engine

MFR - Mass Flow Rate, kg/s

PFI - Port Fuel Injection

RANS - Reynolds Average Navier Stokes

SCR - Selective Catalytic Reduction

© 2025 SAE International and SAE Naples Section. All rights reserved. No part of this publication may be reproduced, stored in a retrieval system, transmitted, in any form or by any means, electronic, mechanical, photocopying, recording, or otherwise, or used for text and data mining, AI training, or similar technologies, without the prior written permission of SAE.

Positions and opinions advanced in this work are those of the author(s) and not necessarily those of SAE International. Responsibility for the content of the work lies solely with the author(s).

ISSN 0148-7191